Chemiluminescence from the $Ba(^3P)+N_2O \rightarrow BaO(A\ ^1\Sigma^+)+N_2$ reaction: Collision energy effects on the product rotational alignment and energy release

Maximiliano Rossa, Carlos A. Rinaldi, and Juan C. Ferrero[a)]
Centro Láser de Ciencias Moleculares, INFIQC, and Departamento de Fisicoquímica, Facultad de Ciencias Químicas, Universidad Nacional de Córdoba, X5000IUS Córdoba, Argentina

(Received 13 July 2009; accepted 29 December 2009; published online 15 January 2010)

Both fully dispersed unpolarized and polarized chemiluminescence spectra from the $Ba(^3P)+N_2O$ reaction have been recorded under hyperthermal laser-ablated atomic beam-Maxwellian gas conditions at three specific average collision energies $\langle E_c \rangle$ in the range of 4.82–7.47 eV. A comprehensive analysis of the whole data series suggests that the $A\ ^1\Sigma^+ \rightarrow X\ ^1\Sigma^+$ band system dominates the chemiluminescence. The polarization results revealed that the $BaO(A\ ^1\Sigma^+)$ product rotational alignment is insensitive to its vibrational state v' at $\langle E_c \rangle = 4.82$ eV but develops into an strong negative correlation between product rotational alignment and v' at 7.47 eV. The results are interpreted in terms of a direct mechanism involving a short-range, partial electron transfer from $Ba(^3P)$ to N_2O which is constrained by the duration of the collision, so that the reaction has a larger probability to occur when the collision time is larger than the time needed for N_2O bending. The latter in turn determines that, at any given $\langle E_c \rangle$, collinear reactive intermediates are preferentially involved when the highest velocity components of the corresponding collision energy distributions are sampled. Moreover, the data at 4.82 eV suggest that a potential barrier to reaction which favors charge transfer to bent N_2O at chiefly coplanar geometries is operative for most of the reactive trajectories that sample the lowest velocity components. Such a barrier would arise from the relevant ionic-covalent curve crossings occurring in the repulsive region of the covalent potential $Ba(^3P)\cdots N_2O(^1\Sigma^+)$; from this crossing the $BaO(A\ ^1\Sigma^+)$ product may be reached through mixings in the exit channel with potential energy surfaces leading most likely to the spin-allowed $b\ ^3\Pi$ and $a\ ^3\Sigma^+$ products. The variation with increasing $\langle E_c \rangle$ of both the magnitude of the average $BaO(A\ ^1\Sigma^+)$ rotational alignment and the $BaO(A\ ^1\Sigma^+)$ rovibrational excitation, as obtained from spectral simulations of the unpolarized chemiluminescence spectra, consistently points to additional dynamic factors, most likely the development of induced repulsive energy release as the major responsible for the angular momentum and energy disposal at the two higher $\langle E_c \rangle$ studied. The results of a simplified version of the direct interaction with product repulsion-distributed as in photodissociation model do not agree with the observed average product rotational alignments, showing that a more realistic potential energy surface model will be necessary to explain the present results. © *2010 American Institute of Physics*. [doi:10.1063/1.3294880]

I. INTRODUCTION

The reactions of metal atoms with halogen and oxygen-containing molecules in the gas phase aroused a continuing interest for more than 70 years.[1–3] An important dynamical aspect of these electron-transfer reactions concerns the role that internal motion of the molecular partner plays in determining the reaction outcome, especially when oxidant molecules having a small positive or a negative electron affinity are involved. In such circumstances, the electron transfer may be prevented from occurring instantly but it would first require either the stretch of a bond or the bend of an angle connecting to a halogen or an oxygen atom of the molecule to increase its electron affinity to the extent that the charge transfer can proceed.[2]

Direct observation of the coupling between an internal coordinate of the molecular reactant (e.g., bond distance or bond angle) and the approach coordinate of the metal atom in molecular-beam scattering experiments is often hindered by the fact that the time needed for deformation of the neutral molecule is usually much shorter than the collision time. As a consequence, cross sections are completely averaged over the internal degrees of freedom. Over the past two decades, though, a number of full-collision studies of metal atom-oxidant reactions reported on evidence suggesting that internal motion of the molecule imposes strong dynamical constraints on the collision time, particularly at collision energies large enough so that the collision time is lower than the time needed for rearrangement of the molecule or the

[a)]Author to whom correspondence should be addressed. Tel.: +54 351 4334169/80. FAX: +54 351 4334188. Electronic mail: jferrero@mail.fcq.unc.edu.ar.

intermediate collision complex. Reported examples include the finding in the $K+CH_3I \rightarrow KI+CH_3$ reaction studied at hyperthermal collision energies of a pronounced steric effect, of comparable magnitude to that observed at thermal energies,[4] as well as the observation of collision energy effects such as stairlike behavior and forward transition state shifts in the chemiluminescent reactions of $Ca(4s3d\ ^1D_2)$ atoms with HCl and HBr (Ref. 5) and ground-state and electronically excited manganese atoms with a variety of molecules,[6] respectively. For the manganese atom reactions with O_2 and SO_2,[6,7] additional measurements of the average $MnO^*(A\ ^6\Sigma^+, A'\ ^6\Pi)$ product rotational alignments as a function of collision energy provided complementary information about the effect of collision-time constraints on the stereodynamics of these systems.

Related time-scale limitations[2] have been considered in a recent study of the chemiluminescent $Ba(^3P)+N_2O$ reaction under beam-gas conditions at hyperthermal collision energies from this laboratory,[8] to account for the observed negative correlation between the rotational alignment of the $BaO(A\ ^1\Sigma^+)$ product and its vibrational level. Such behavior has been rationalized by assuming that the reaction involves a short-range, partial electron transfer from $Ba(^3P)$ to N_2O which is constrained by the duration of the collision, so that the reaction has a larger probability when the N_2O has time enough to bend during the collision. This dynamical aspect of the reaction was deemed to be of utmost importance given that the hyperthermal, laser ablation $Ba(^3P)$ atom source used there has a broad distribution of collision energies, thus reflecting a wide range of collision times. This in turn is expected to result in specific generation of products in relatively low v' levels and with substantial center-of-mass alignment from reactive encounters that sample the highest velocity components of the collision energy distribution, and the opposite tendency, or a lack of specificity whatsoever, in the low collision energy regime.

This article reports an extended study of the $Ba(^3P)+N_2O \rightarrow BaO^*+N_2$ reaction dynamics under beam-gas conditions. Advantage was taken here of the ability to modify significantly the $Ba(^3P)$ velocity distribution by changing the laser ablation conditions of the atomic beam source used previously.[8–10] Average values for both the initial relative velocity and collision energy that have been reported in Ref. 8, where pure thermal conditions were erroneously assumed are recalculated here by applying a different procedure, which is appropriate to the present hyperthermal atomic beam-Maxwellian gas experiments. The analysis of both unpolarized and polarized BaO chemiluminescence spectra and their average collision energy dependence supports the previous assignment of the emission to the $A\ ^1\Sigma^+ \rightarrow X\ ^1\Sigma^+$ band system. Average and wavelength-resolved values of the product rotational alignment associated with the parallel $BaO(A\ ^1\Sigma^+ \rightarrow X\ ^1\Sigma^+)$ emission are presented for the two specific average collision energies of 4.82 and 7.47 eV. $BaO(A\ ^1\Sigma^+)$ rovibrational population distributions at the average collision energies of 4.82, 5.85, and 7.47 eV are also determined by simulating the corresponding unpolarized chemiluminescence spectra. Taken altogether, the results provide a comprehensive picture of the energy and angular momentum disposal in the title reaction. Attempts to account for the observed average product rotational alignments by using a simplified version[11] of the generalized electron-jump direct interaction with product repulsion-distributed as in photodissociation (DIPR-DIP) model[12] provided further clues to the major dynamic factors controlling the angular momentum disposal at the hyperthermal collision energies studied.

II. EXPERIMENT

The experimental setup and procedure are essentially as described before.[8] Briefly, a 5 Hz pulsed Ba atom beam was generated by focusing the 1064 nm output of a *Q*-switched neodymium:yttrium aluminum garnet laser (Laseroptics LND 532, 10 ns) onto a rotating Ba disk at normal incidence in high vacuum conditions. The ablation laser fluence ϕ was set to the three specific values of 5.3, 7.6, and 10.8 J/cm^2 with an approximately 0.25 mm diameter laser spot. The ablated material passed through a 0.2 cm diameter collimator, located 0.3 cm from the ablation volume, into a 6 cm length scattering cell. A detailed characterization of the resulting beam at the prevailing laser ablation conditions and in the absence of N_2O scattering gas has been reported elsewhere.[8–10] The time-of-flight (TOF) technique through pulsed laser-induced fluorescence and time-resolved fluorescence detection was used to this goal. At 3.3 cm from the Ba disk surface where the chemiluminescence is probed, the barium beam is composed mainly of neutral atoms in the $6s^2\ ^1S_0$, $6s5d\ ^3D_J$, and $6s6p\ ^3P_J$ states in an overall abundance >98% of that of the total Ba atoms. The approximate beam compositions regarding these relevant Ba atom states at the three ablation conditions are listed in Table I. These were determined by numerically integrating the whole TOF profiles of the $^1S_0$, ^3D_J, and ^3P_J states of Ba[8–10] and further processing the resulting areas as described in Ref. 8. The corresponding TOF distributions are broad and bimodal; increasing ϕ from 5.3 to 10.8 J/cm^2 was found to modify significantly the general form of the TOF distributions of $^3P_1$, but to alter hardly the shape and peak of those corresponding to $^1S_0$ and ^3D_J. The flux-weighted $Ba(^3P_1)$ TOF distributions, corrected also for the metastable radiative decay of the $^3P_1$ state ($A=3.53\times10^5\ s^{-1}$),[13] were fitted to a superposition of two terms of a two-parameter form for the velocity distribution $f(v)=Nv^3 \exp[-(v-v_0)^2/\alpha^2]$, where v denotes the velocity, N is a normalization constant, and v_0, α are adjustable parameters. Table II shows the parameters obtained from the best fits, together with values of the average initial relative velocity $\langle k \rangle$ and collision energy $\langle E_c \rangle$ for both the two components and the whole of the velocity distributions of $Ba(^3P_1)$, as derived from convoluting[14] the beam and target N_2O (298 K) gas distributions. Note that the procedure used here to derive $\langle k \rangle$ and $\langle E_c \rangle$, which takes v_0 into account, is different from that used previously,[8] where pure thermal conditions were erroneously assumed. In the present, proper approach the values of $\langle k \rangle$ and $\langle E_c \rangle$ at 7.6 J/cm^2 are found to be (5.8 ± 0.4) km/s and (5.85 ± 0.04) eV, respectively. While other components of the ^3P level have not been investigated, their velocity distributions should be very similar to that for $^3P_1$, as it was found previously for ^3D_J.[9,10] The

TABLE I. Reactant Ba beam compositions in percent of the most populated $6s^2\ ^1S_0$, $6s5d\ ^3D_J$, and $6s6p\ ^3P_J$ electronic states of Ba atoms. For each laser ablation fluence reported, the experimental values probing the $^3P_1$ substate alone are given in the left column, while values (in italics) in the right column are rough estimates (see Ref. 8 for details) of the overall compositions including the relative contribution of the $^3P_{0,2}$ states, as computed by assuming $2J+1$ degeneracies at the ablation volume and properly accounting for Ba(^3P_J) radiative decay over the flight path.

State	Excitation energy (eV)	Fluence (J/cm^2) 5.3		7.6		10.8	
Ba($^1S_0$)	0	65.8 ± 5.3	*51.3*	71.4 ± 5.7	*48.4*	82.4 ± 6.6	*57.9*
Ba(^3D_J)	1.16	28.6 ± 1.9	*22.3*	19.1 ± 1.5	*13.0*	9.2 ± 0.7	*6.4*
Ba($^3P_1$)	1.57	5.6 ± 0.4	⋯	9.4 ± 0.6	⋯	8.4 ± 0.6	⋯
Ba(^3P_J)	1.62	⋯	*26.4*	⋯	*38.6*	⋯	*35.7*

amount of small Ba_n species in the beam is considered to be negligible since neither laser-induced fluorescence nor emission other than those of monatomic Ba species were detected.

For chemiluminescence experiments, the atomic beam was allowed to interact within the scattering cell with a standing pressure of N_2O (AGA, 99.8%, 0.76 mTorr). The chemiluminescence from reactive collisions was collected perpendicularly to the beam axis at 3.3 cm from the disk surface by a biconvex lens and analyzed by the same scanning monochromator and photomultiplier tube combination as in Ref. 8, which was operated with a resolution of 0.5 nm. Signals from four laser shots were averaged and time integrated from the firing of the ablation laser to extinction for each spectral point. For polarization measurements, a visible linear polarizer (Edmund Optics, 52–557) was placed between the collecting lens and the monochromator. This linear polarizer was rotated in order to measure the chemiluminescence polarized in the planes perpendicular and parallel to the direction of the Ba beam. Since the contribution of the most populated Ba ($^1S_0$, ^3D, and ^3P) states to the chemiluminescence spectra is dominant under these conditions, the spectra corresponding only to the collision of Ba(^3P_J) with N_2O were determined by subtracting the joint contribution of the $^1S_0$ and ^3D_J states, in much the same way as the polarized Ba(^3P)+N_2O chemiluminescence spectra were previously obtained.[8] The effect of the ionic species present in the beam was neglected since their removal, by a pair of deflection plates, did not significantly affect the observed chemiluminescence spectra.

TABLE II. Parameters that characterize both the two components and the whole of the Ba($^3P_1$) velocity distributions in the reactant atomic beam, together with the corresponding average values for the initial relative velocity and collision energy distributions in the beam-gas scattering experiments. Raw data at ϕ=7.6 J/cm^2 were taken from previous work (Ref. 8).

Fluence (J/cm^2)	Parameter	Component Slow	Fast
5.3	N	$(9,15 \pm 0,05) \times 10^{-21}$	$(1,364 \pm 0,001) \times 10^{-21}$
	v_0(km/s)	1.8 ± 0.2	4.8 ± 0.2
	α^2(m^2/s^2)	$(164 \pm 2) \times 10^3$	$(3540 \pm 7) \times 10^3$
	$\langle k \rangle_i$(km/s)	1.9 ± 0.4	5.7 ± 0.2
	$\langle k \rangle$(km/s)	5.3 ± 0.3	
	$\langle E_c \rangle_i$(eV)	0.65 ± 0.05	5.52 ± 0.03
	$\langle E_c \rangle$(eV)	4.82 ± 0.04	
7.6	N	$(3,93 \pm 0,02) \times 10^{-21}$	$(1,279 \pm 0,004) \times 10^{-21}$
	v_0(km/s)	1.8 ± 0.1	4.4 ± 0.1
	α^2(m^2/s^2)	$(254 \pm 4) \times 10^3$	$(651 \pm 3) \times 10^4$
	$\langle k \rangle_i$(km/s)	2.0 ± 0.3	6.1 ± 0.6
	$\langle k \rangle$(km/s)	5.8 ± 0.4	
	$\langle E_c \rangle_i$(eV)	0.70 ± 0.05	6.29 ± 0.04
	$\langle E_c \rangle$(eV)	5.85 ± 0.04	
10.8	N	$(1,81 \pm 0,01) \times 10^{-21}$	$(2,225 \pm 0,005) \times 10^{-21}$
	v_0(km/s)	1.6 ± 0.9	3.3 ± 0.8
	α^2(m^2/s^2)	$(97 \pm 2) \times 10^4$	$(1361 \pm 2) \times 10^4$
	$\langle k \rangle_i$(km/s)	2.2 ± 0.4	6.7 ± 0.4
	$\langle k \rangle$(km/s)	6.6 ± 0.3	
	$\langle E_c \rangle_i$(eV)	0.86 ± 0.03	7.68 ± 0.03
	$\langle E_c \rangle$(eV)	7.47 ± 0.03	

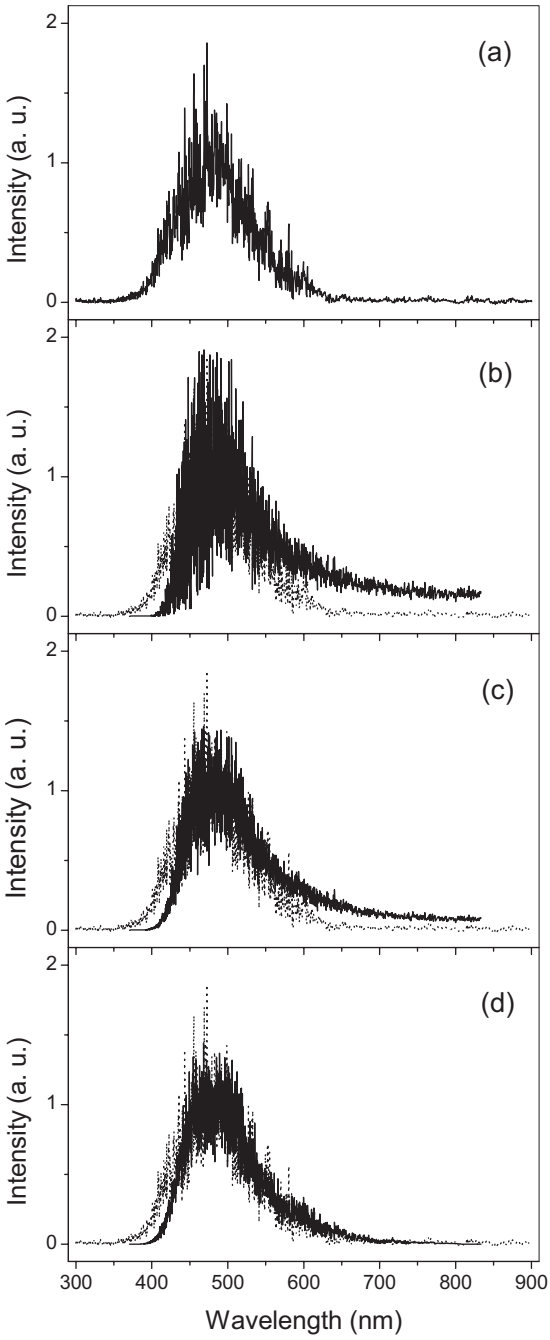

FIG. 1. (a) $Ba(^3P)+N_2O$ chemiluminescence spectrum recorded at a N_2O pressure of 0.76 mTorr and at $\langle E_c\rangle=7.47$ eV. It represents the average of three individual scans previously corrected by spectral response of the detection system (Ref. 8). (b), (c), and (d) compare the experimental spectrum (···) to simulations (—) of BaO $A\ ^1\Sigma^+$ and $A'\ ^1\Pi$ emission using electronic branching ratios $\Gamma(A/A')$ of 0, 1, and ∞, respectively.

III. RESULTS AND ANALYSIS

A. Chemiluminescence spectra

The shapes of the $Ba(^3P)+N_2O$ chemiluminescence spectra were quite similar for the three average collision energies used in this work, and Figure 1(a) shows a representative unpolarized spectrum obtained at $\langle E_c\rangle=7.47$ eV. Increasing $\langle E_c\rangle$ from 4.82 to 7.47 eV was found to cause a comparatively minor shift in wavelength from 479 to 486 nm of the peaks of such spectra where no molecular band systems are discernible. Although a detailed spectroscopic assignment is not feasible here, a consideration of the $Ba(^1S_0,^3D)+N_2O$ chemiluminescence spectra under beam-scattering conditions can help in identifying spectral features. In both lower-excited reaction channels, unstructured, broad spectra over the near-ultraviolet/visible/near-infrared range have been observed and ascribed to dominant joint $A\ ^1\Sigma^+\rightarrow X\ ^1\Sigma^+$ and $A'\ ^1\Pi\rightarrow X\ ^1\Sigma^+$ emission; for the $Ba(^3D)$ reaction, a feature in the red near 800 nm was also observed and assigned to the $D\ ^1\Sigma^+\rightarrow A\ ^1\Sigma^+$ transition.[15,16] Noteworthy is the limited number of BaO luminescent states that are observed in these lower-excited reactions regarding the whole electronic states that are energetically accessible. Indeed, the complete ground state $Ba+N_2O\rightarrow BaO+N_2$ reaction is already significantly exoergic ($\Delta D^0=-4.11$ eV) so that all presently known electronic states of BaO 14 in number at energies ≤4.29 eV (Refs. 17–21) could be populated at the range of thermal collision energies of previous studies.[15,16] Generation of several thus far unobserved excited states, such as the Δ states that are expected to lie in the 2–4 eV range on the basis of indirect spectroscopic evidence,[17,18] may be partially the cause for the apparent predominance of the A and A' states of BaO in the chemiluminescent $Ba(^1S_0,^3D)+N_2O$ reactions.[15]

At the hyperthermal $\langle E_c\rangle$ studied here, the $Ba(^3P)+N_2O$ chemiluminescence is concentrated over the 400–600 nm spectral region and does not exhibit the red feature seen in the corresponding $Ba(^3D)$ reaction. Since the emission here lies within the wavelength region (~350–900 nm) covered by the $A-X$ and $A'-X$ systems of BaO,[22] one or both of the latter, and arguably also the $a\ ^3\Sigma^+\rightarrow X\ ^1\Sigma^+$ transition,[23] could be involved in much of the observed chemiluminescence, as it was found to be the case for the related Ba ($^1S_0$, ^3D, $^1D_2$, and $^1P_1$) reactive channels.[15,16,24] Nevertheless, the long radiative lifetimes of the $A'\ ^1\Pi(\tau=9\ \mu s)$ (Ref. 25) and the triplet (metastable) states make drift of these excited BaO products out of the detector field of view sizeable at the hyperthermal average initial relative velocities of the present experiments. Indeed assuming that the product velocity in the laboratory frame is comparable to $\langle k\rangle$, a BaO molecule will travel 47.7 mm during 9 μs for the average velocity of 5.3 km/s at $\langle E_c\rangle=4.82$ eV. This is about nine times the diameter (~5.3 mm) of the observation volume for the present experiments,[8] and higher ratios would be clearly obtained in the case of the triplet states. In contrast, a similar calculation performed for the short-lived ($\tau=350$ ns) (Ref. 26) $A\ ^1\Sigma^+$ state leads to a travel distance of 1.9 mm. Thus, as far as the BaO states lying in the 2 eV region are concerned,[18,20] the optics detection system used here was likely to be sensitive mainly to the $A\ ^1\Sigma^+$ state. Both spectral simulation of the BaO chemiluminescence and the polarized $Ba(^3P)+N_2O$ chemiluminescence spectra to be reported in Secs. III B and III C, respectively, will add evidence for the predominance of the $A-X$ transition over $A'-X$ and $a-X$.

The BaO states lying above 4 eV (Refs. 17 and 19) may also contribute to the observed emission via transitions to either the ground state or lower-lying excited states. Of the many possible systems, quite a few have been actually docu-

mented in the visible range, namely, $C\ ^1\Sigma^+-a$, A, $b\ ^3\Pi_1$, A', and the weaker portion of $C\ ^1\Sigma^+-X$,[17,19,27] by means of a number of laser spectroscopies. Other band systems have been reported in the UV range and ascribed to the $C-X$ transition,[27] along with the above-mentioned chemiluminescent feature near 800 nm that was assigned to $D-A$ emission.[15] Neither of the latter are in evidence here [Fig. 1(a)]. At least for the $C-X$ emission, flyout effects would not be of significance given the short radiative lifetime (τ =10.5 ns) (Ref. 28) of the $C\ ^1\Sigma^+$ state. The absence here of UV emission associated with the $C-X$ system parallels observations made previously in the Ba(^3D)+N_2O reaction.[15] Such findings were suggested there as an argument against a $C-A$, A' contribution to the 800 nm feature as these emissions, if present, would be expected to be one order of magnitude weaker than $C-X$.[28] Clearly, the contribution of $C-A$, A' emission to the chemiluminescence here can be dismissed on similar grounds.

Concerning the involvement here of 4 eV states other than C and D as emitters, no definite assessment could be made given that the dipole transition moments for the prospective band systems are unknown. An insight can still be gained on the basis of calculated Franck–Condon factors (FCFs). Such calculations are feasible for six out of seven remaining high-lying states, which have been sufficiently well characterized to permit construction of potential energy curves.[19] These are, in order of increasing energy, $B\ ^1\Pi$, $E\ ^1\Sigma^+$, $F\ ^3\Pi_1$, $c\ ^3\Pi_0$, $G\ ^3\Pi_0$, and $H\ ^3\Pi_1$. FCFs were obtained using numerical potentials generated by the Rydberg–Klein–Rees (RKR) method[29] of inverting spectroscopic data via the RKR1 and LEVEL program packages.[30] The relevant spectroscopic constants for all systems terminating on the ground state were taken from Refs. 19 and 31; FCF were then calculated for transitions from $v' \leq 10$ to $v'' \leq 34$. For all six possible systems, the magnitude of the FCF for any given (v', v'') pair is quite similar, the largest FCF (≥ 0.05) occurring generally in the 270–670 nm wavelength range. Neither of the relevant systems have been observed in shock tube absorption between 290 and 390 nm,[32] which implies that the corresponding transition moments are probably small. This, combined with the fact that no chemiluminescence is found here at wavelengths less than 362 nm suggests that the $B,E,F,c,G,H-X$ systems are unlikely to contribute to the observed emission.

FCFs were also calculated for all 24 possible band systems involving transitions from $v' \leq 10$ of the B, E, F, c, G, and H states to $v'' \leq 34$ of the lowest excited a, A, b, and A' states.[18] For both a/A and b/A' pairs, it is found that the FCF matrices corresponding to any given higher-lying state are almost identical, as expected from the near degeneracy of the relevant triplet/singlet states within the range of v'' considered. There are significant differences between the FCF matrixes for transitions terminating, on one hand, on a/A states as well as the $H-b/A'$ transitions, which have the largest FCF (0.05–0.30) for wavelengths greater than 500 nm, and on the other hand, on the remaining b/A' states having strong FCF (≥ 0.1) generally in the more limited wavelength range of 600–800 nm. In all cases the FCFs vanish for wavelengths less than 500 nm. Taken altogether, the results allow for broad emission above 500 nm and into the near-infrared to be expected from the various $B,E,F,c,G,H-a,A,b,A'$ band systems. Indeed, the FCF matrices for $G,H-a,A$ transitions bear a remarkable similarity to that for the $D-A$ system, on which assignment[15] as $D-A$ emission of the broad feature at 750–890 nm that is observed in the Ba(^3D)+N_2O reaction was mainly based. The E, F, G, and H states were unknown, and both B and c states were incompletely characterized at the time of Cox and Dagdigian's report,[15] but it is clear from the present evidence that $B,E,F,c,G,H-a,A$ as well as the $H-b/A'$ emission may well account for such broad red feature. The lack of observation of chemiluminescence at wavelengths greater than 650 nm instead indicates that $B,E,F,c,G,H-a,A,b,A'$ emission is not present here. This reinforces suggestions made in the two preceding paragraphs that, under the present experimental conditions, the emitter is unlikely to be one of the known states at 4 eV. Nevertheless, it is entirely possible that presently unknown either singlet or triplet BaO excited states lying at energies $\leq$4.29 eV could be responsible for the observed chemiluminescence.

The Ba(^3P)+N_2O reaction is 1.62 eV above the ground state channel, which, given the BaO ionization energy of 6.91 ± 0.06 eV,[33] would allow population of excited states of BaO much higher in energy than those hitherto considered including Rydberg states. However, the latter are not likely to emit strongly in the visible but instead expected to radiate by a cascade mechanism, the initial steps of which will involve Rydberg–Rydberg transitions at long wavelength. Corroboration of the presence of such highly excited BaO states would clearly require detection of chemiluminescence at wavelengths in the IR range, which, unfortunately, is out of the sensitive spectral range of the detection system used here. In addition, the total energies available to the BaO products E_{tot} at the prevailing $\langle E_c \rangle$, as listed in Table III are extremely high and would allow formation of nonemitting products from both collision-induced dissociation $Ba+N_2O \rightarrow Ba+O+N_2$ as well as collisional ionization $Ba+N_2O \rightarrow Ba^+ + N_2O^-$.

Thus, both the present experimental observations and most of the available spectroscopic information consistently suggest that, under the present conditions, the observed Ba(^3P)+N_2O chemiluminescence spectra are dominated by $A\ ^1\Sigma^+ \rightarrow X\ ^1\Sigma^+$, and probably also $A'\ ^1\Pi \rightarrow X\ ^1\Sigma^+$ emission. Spectral simulations of the BaO emission, to be described next, were tried in order to substantiate such an assignment, while also allowing to extract the nascent BaO* product state distributions from the experiments.

B. Spectral simulations

A number of tests has been performed by varying the input A and A' rovibrational distributions as well as the electronic branching ratio $\Gamma(A/A')$ in the simulation program. The relevant spectroscopic constants were taken from Gottscho *et al.*;[18] at the present spectral resolution and extensive internal excitation of the products (see below), though, it was found that the use of more recent, improved constants reported by Furio and Pruett[20] for the excited state

TABLE III. Energy disposal in the $Ba(^3P)+N_2O \rightarrow BaO^*+N_2$ reaction at the various average collision energies. All energy values are in eV.

						Observed blue limit E_B		
$\langle E_c \rangle$	E_{tot}[a]	E_{vib}^{MPb}	E_{vib}^{Maxb}	$\langle E_{rot} \rangle^{b,c}$	E_d[d]	λ(nm)	E_B	$E_{tot}-E_B$
4.82	10.55	0, 54	1, 79	0, 22	6.46	364	3.41	7.14
5.85	11.58	0, 54	1, 79	0, 22	7.49	362	3.43	8.15
7.47	13.20	0, 54	1, 79	0, 22	9.11	362	3.43	9.77

[a]Reaction exoergicity plus average collision energy.
[b]These quantities refer to the internal energy of the BaO product alone, as derived from the best fits to the experimental spectra using $v'^{MP}=9$, $v'^{Max}=34$, and $\langle J' \rangle=91$.
[c]Value at $v'^{Max}=34$ of $BaO(A\ ^1\Sigma^+)$.
[d]Taken above T_e for the $A\ ^1\Sigma^+$ state of BaO.

and Li *et al.*[21] for the ground state did not lead to noticeable differences regarding the results that derive from the preferred set of constants. FCFs for the $A-X$ and $A'-X$ band systems were obtained by the procedure described in Sec. III A. The rotational line strengths were taken from Herzberg.[34]

It follows from preliminary simulations including either excited electronic state that a substantial BaO rotational excitation, characterized by a rotational temperature T_r in the range of 3000–4000 K, is required to reproduce the headless, "many-line" appearance of the experimental spectra [see Fig. 1(a)]. This allows one to yield only an estimate of the mean rotational excitation of the BaO^* products. In the recorded wavelength region, though, the corresponding input vibrational distributions are found to have a much more marked effect on the envelops of the simulated spectra. Such findings are in good agreement with conclusions reached in a previous study[35] of the $Ba(6s6p\ ^1P_1)+CO_2$ reaction at a number of thermal collision energies and, as there, they afforded here to extract reliable information about the BaO^* vibrational excitation from the fits.

Further inspection of the effect of the A/A' branching ratio on the simulations leads to the conclusion that the red part ($\lambda > 700$ nm) of the calculated spectra is very sensitive to this parameter, again in accord with previous findings for the $Ba(6s6p\ ^1P_1)+CO_2$ reaction.[35] This feature was found to be advantageous here in order to ascertain the relative $A-X$ and $A'-X$ contribution to the observed emission. Thus, Figures 1(b)–1(d) compare the experimental spectrum at $\langle E_c \rangle = 7.47$ eV with three examples of simulated spectra corresponding to different values for Γ. The input, inverted vibrational distributions used for the A and A' states are shown in Figure 2. For the rotation motion, Boltzmann distributions characterized by $T_r=4000$ and 3000 K were chosen for the A and A' states, respectively. It is readily apparent from Fig. 1 that the most satisfactory agreement between calculation and experiment is obtained in the case of pure A contribution, i.e., $\Gamma=\infty$. There are only slight discrepancies in the blue wing of the chemiluminescence, particularly in the region below 430 nm where the calculated spectrum decreases to extinction much faster than observed. It should be noticed that such discrepancies remain whatever the value of Γ as well as the chosen A and A' rovibrational distributions. Before addressing this concern, it is important to highlight at this stage that addition of any A' contribution differently affects the red wing of the simulated spectra, which then dye off toward the red much slowly than both the experiment and the pure A calculation, and extends beyond 850 nm. The fact that no signal is experimentally observed here at $\lambda > 650$ nm allows to state that such $A'-X$ emission, if present, contributes only to the background level. Indeed, an $A-X$ to $A'-X$ intensity ratio of 99/1 could be estimated under the present conditions from the observed 40:1 signal-to-noise ratio [see Fig. 1(a)], which can be taken as a further evidence for a predominant $A-X$ contribution. Actually, these conclusions hold irrespective the average collision energy considered since the marked similarity among the corresponding chemiluminescence spectra resulted in the same $A-X$ simulation parameters leading to a satisfactory fit.

In tracing the possible sources of the blue wing discrepancies, there is to note that inclusion of either $a\ ^3\Sigma^+$ or $b\ ^3\Pi$ states in the simulations is not expected[36] to lead to noticeable differences regarding the case for the contribution of only A and A' states, since these corresponding triplet and singlet states cannot be resolved in the present experiments.

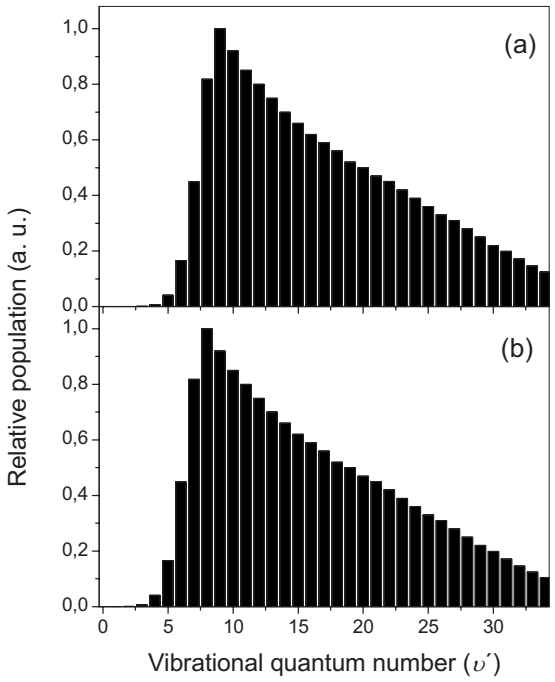

FIG. 2. Vibrational state distributions of the (a) $A\ ^1\Sigma^+$ and (b) $A'\ ^1\Pi$ electronic states of BaO products corresponding to the simulations of Fig. 1.

Moreover, any possible $a-X$ and $b-X$ contributions to the observed emission are deemed to be even less than that of $A'-X$ as a result of stronger flyout effects that are expected on the metastable triplet products with respect to the shorter-lived A' state. From the discussion in Sec. III A, it is also clear that, while any definite conclusion about the contribution of higher-lying BaO states is virtually impossible, it is highly unlikely for one of the known states at 4 eV to be the emitter, and thus being responsible for such discrepancies. Instead, an examination of the vibrational levels v' of the $A\ ^1\Sigma^+$ state that have the largest FCF for fluorescence emission to the $X\ ^1\Sigma^+$ ground state at a given wavelength can be helpful [see Fig. 4(b) of Ref. 8]. It reveals[8] that the main contribution to the chemiluminescence spectrum below 430 nm originates from fairly large BaO($A\ ^1\Sigma^+$) vibrational quantum numbers ($v' \geq 20$) while emission above 540 nm is dominated by molecules with low vibrational excitation ($v' \leq 8$). Actually, the determination by the RKR method of the corresponding FCF for $v' > 20$ may be rather uncertain owing to the extrapolation of the relevant potential curves to vibrational and rotational states much higher in energy than those from which the input spectroscopic constants of Ref. 18 have been obtained. This would lead in turn to a substantial uncertainty in the calculated emission intensity of such blue chemiluminescence wing, which might be the cause of the disagreement. Nonetheless, the best-fit simulation considering BaO($A\ ^1\Sigma^+$) as the sole emitter [see Fig. 1(d)] generally reproduces the main features of the experiment, namely, the envelope of the spectrum and the amplitude of its "noise," which indicates that both the vibrational distribution and the average rotational energy used in the calculation should be close to the real ones.

Essentially the same simulation parameters are appropriate to fit the chemiluminescence spectra at all $\langle E_c \rangle$, which means that the internal energy of BaO* remains almost constant as the collision energy is increased. An upper limit to such internal energy can be obtained by adding together the value of energy E_{vib}^{Max} corresponding to the highest populated vibrational level of the BaO($A\ ^1\Sigma^+$) product resulting from the best fits and the corresponding mean rotational energy $\langle E_{rot} \rangle$. Both values are listed in Table III, along with the difference E_d between the total energy available to the BaO($A\ ^1\Sigma^+$) products E_{tot} and these values. Although E_d only yields a lower limit to the energy released as translation and as internal energy of the N_2 fragment, values in Table III show up a substantial gap between the internal energy of most of the BaO($A\ ^1\Sigma^+$) products and the total product energy in the title reaction.

Alternatively, a piece of information regarding energy disposal could be obtained from the short-wavelength limit of the observed chemiluminescence spectra,[15] which is largely independent of a definite spectroscopic assignment of the emitters. The blue limits at all $\langle E_c \rangle$ are also listed in Table III, where the corresponding photon energies are compared with the total product energy. It is worth noting the close agreement between the values for $E_{tot}-E_B$ and E_d at every $\langle E_c \rangle$, which represent two ways of estimating the energy deficit in the present reaction, while also constituting separate evidence for a main BaO($A\ ^1\Sigma^+$) emitter.

C. Polarized chemiluminescence spectra and product rotational alignment

Figure 3(a) presents the parallel and perpendicular polarized spectra at $\langle E_c \rangle = 4.82$ and 7.47 eV, from which a reduction in the sensitivity of the emission band as a whole to the polarization direction can be ascertained at the highest $\langle E_c \rangle$. To make this evident, the degree of polarization, defined by the expression

$$P = \frac{I_\parallel - I_\perp}{I_\parallel + I_\perp}, \tag{1}$$

was obtained as a function of wavelength from the chemiluminescence intensities polarized parallel, $I_\parallel$, and perpendicular, $I_\perp$, to the barium beam axis, and it is shown at the two working $\langle E_c \rangle$ in Fig. 3(b). Comparison with the corresponding data at 5.85 eV (see Fig. 4 of Ref. 8; there, $\langle E_c \rangle$ was erroneously calculated to be 1.56 eV) shows that the values of P at any given emission wavelength decrease with increasing $\langle E_c \rangle$, which is confirmed by the average polarization values associated with the whole BaO* emission that are listed as a function of $\langle E_c \rangle$ in Table IV. The BaO* polarization at 7.47 eV is also found to increase with wavelength by more than a factor of 25 over the whole emission band, which is in line with, but significantly higher than the approximately fivefold increase in the P values that was previously observed at 5.85 eV.[8] This does not appear to be the case at 4.82 eV, where no discernible emission wavelength dependence of the P values is observed throughout the emission band.

As made in the preceding two sections, it is also important here to consider the possibility that two or more BaO excited states are responsible for the observed (polarized) emission. In such a case, whereas the individual contributions to $I_\parallel$ and $I_\perp$ would be additive, the very definition of P implies that the corresponding contributions to the observed degree of polarization cannot be resolved in individual terms. Nevertheless, some predictions about the effect on P of individual contributions as a function of $\langle E_c \rangle$ could still be made in the case of the two overlapping $A-X$ and $A'-X$ band systems, which are associated with electronic transitions with dominant parallel and perpendicular character, respectively. The latter guarantees that a bias to positive values of P have to ensue any increasing $A-X$ contribution to the emission, while the opposite will be true for an increasing $A'-X$ contribution. Under the present conditions, any prospective $A'-X$ contribution to the polarized spectra is anticipated to decrease with rising $\langle E_c \rangle$, with an accompanying increase in the bias of P at any given emission wavelength to positive values owing to flyout effects for the longer-lived $A'\ ^1\Pi$ state, which is contrary to the present observations [see Fig. 3(b)]. The situation would become tremendously more intricate in the case that additional parallel or perpendicular transitions are contributing to the polarized emission. Notwithstanding, the rather smooth dependence of $P(\lambda)$ observed throughout the emission band at all $\langle E_c \rangle$ studied indicates that there should be only a very small number of BaO excited states that contribute to the chemiluminescence. Most of the evidence presented above in analyzing the un-

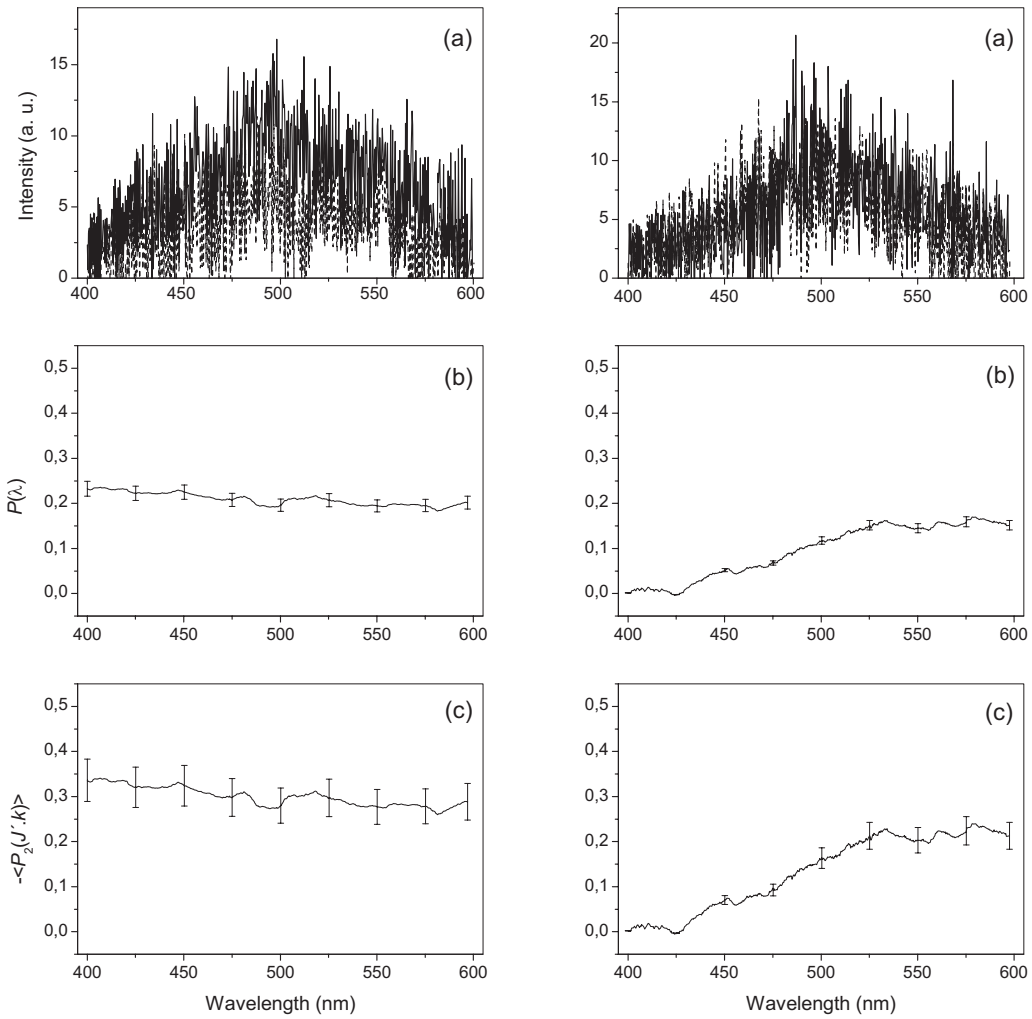

FIG. 3. (a) Ba(^3P)+N_2O chemiluminescence spectra polarized parallel (—) and perpendicular (---) to the Ba beam axis at a N_2O pressure of 0.76×10^{-3} Torr. Each represents the average of three individual scans previously corrected by spectral response (including instrumental polarization) (Ref. 8). (b) Degree of polarization of the BaO($A\ ^1\Sigma^+$) chemiluminescence as a function of wavelength, λ. Three consecutive λ values were binned so that the resolution was ~1.5 nm; the error bars thus reflect the average intensity uncertainty. (c) BaO($A\ ^1\Sigma^+$) product rotational alignment as a function of wavelength. Left and right panels correspond to the average collision energies of 4.82 and 7.47 eV, respectively.

polarized spectra and their spectral simulations certainly suggest that the $A-X$ band system does dominate chemiluminescence. Hence, the ensuing analysis of the corresponding polarized spectra will be based on assuming that such parallel transition is solely responsible for the emission here.

The center-of-mass product rotational alignment $\langle P_2(J'\cdot\hat{k})\rangle$ was extracted from the polarization measurements. For a parallel-type transition, P and the value of $\langle P_2(J'\cdot\hat{k})\rangle$ are related by the expression[37]

$$\langle P_2(J'\cdot\hat{k})\rangle = \frac{-4P}{3-(P\cdot\langle P_2(\hat{k}\cdot z)\rangle)}, \tag{2}$$

where the term $\langle P_2(\hat{k}\cdot z)\rangle$ properly accounts for the beam-gas averaging, and z is along the beam axis. In the present experimental configuration, $\langle P_2(\hat{k}\cdot z)\rangle$ depends on the masses of the beam and gas species, the temperature of the latter and the nominal collision energy ($E_c^0=(1/2)\mu(x/t)^2$) through one reduced parameter.[38] As shown previously,[8] it is reasonable to assume that $\langle P_2(\hat{k}\cdot z)\rangle\sim1$ for the reactive collision energies employed in the present experiments. Figure 3(c) displays the conversion of the $P(\lambda)$ data presented in Fig. 3(b) to $\langle P_2(J'\cdot\hat{k})\rangle(\lambda)$ by means of Eq. (2), and Table IV contains the BaO($A\ ^1\Sigma^+$) rotational alignment values averaged throughout the emission band $\langle P_2(J'\cdot\hat{k})\rangle_{av}$ at all working $\langle E_c\rangle$. Note that the latter are close to the range of values of $-\langle P_2(J'\cdot\hat{k})\rangle=0.14-0.38$ (Refs. 39 and 40) and 0.33 (Ref. 40) previously reported for the Ba($^1S_0$)+N_2O and Ba(^3D)+N_2O reactions, respectively, which were also studied under beam-gas conditions but at a range of thermal collision en-

TABLE IV. Experimental average degree of polarization and product rotational alignment for the whole parallel BaO($A\ ^1\Sigma^+\rightarrow X\ ^1\Sigma^+$) emission at the various average collision energies. Data at $\langle E_c\rangle=5.85$ eV were taken from previous work (Ref. 8); note that $\langle E_c\rangle$ there was erroneously calculated to be 1.56 eV. Also shown are theoretical values for the product rotational alignment that derive from a DIPR-DIP calculation (Ref. 11).

$\langle E_c\rangle$ (eV)	Experimental			Calculated
	P	$\langle P_2(\hat{k}\cdot z)\rangle$	$\langle P_2(J'\cdot\hat{k})\rangle$	$\langle P_2(J'\cdot\hat{k})\rangle$
4, 82	0.20±0.01	1	−0.29±0.03	−0.28
5, 85	0.15±0.01	1	−0.21±0.03	−0.31
7, 47	0.09±0.02	1	−0.12±0.04	−0.34

ergies. Clearly the BaO($A\ ^1\Sigma^+$) product is significantly aligned at the hyperthermal collision energies studied here and, in spite of the limited number of data, it is apparent that the average product rotational alignment decreases with increasing $\langle E_c \rangle$. Taken altogether, the data presented here and elsewhere[8] reveal an additional trend in the variation of the BaO($A\ ^1\Sigma^+$) rotational alignment with collision energy: While the $\langle P_2(J' \cdot \hat{k}) \rangle$ values are rather insensitive to the emission wavelength at 4.82 eV, a marked wavelength dependence of $\langle P_2(J' \cdot \hat{k}) \rangle$ is observed at 5.85 and 7.47 eV which becomes more pronounced as $\langle E_c \rangle$ rises [cf. Fig. 4(c) of Ref. 8 and Fig. 3(c) of the present work). Once again looking at the largest FCFs for the $A\ ^1\Sigma^+ \rightarrow X\ ^1\Sigma^+$ transition, it is apparent that the behavior at the highest $\langle E_c \rangle$s studied here can ascribed to a tendency for BaO($A\ ^1\Sigma^+$) rotational alignment to be negatively correlated with BaO* vibrational levels. Such behavior was not reported in previous studies of the lower-excited reaction channels.[39,40]

IV. DISCUSSION

Two features of the present observations concerning the effect of the average collision energy in the 4.82–7.47 eV range on the Ba(^3P)+N_2O reaction are most distinctive: the little discernible variation of the shapes of the chemiluminescence spectra with increasing $\langle E_c \rangle$ and the far more marked $\langle E_c \rangle$ dependence of the average and wavelength-resolved degrees of polarization associated to the BaO* emission. The former strongly suggests that the number of BaO* emitters as well as their internal energy remain nearly constant as $\langle E_c \rangle$ is increased. This may be unsurprising given that the total product energy at the lowest $\langle E_c \rangle$ studied here is already significantly higher than the BaO ionization energy, below which the BaO emitting levels are bound to lie, so that the additional collision energy is not as dramatic an increase in E_{tot}. Admittedly that it is possible for the lower collision energy components of the whole E_c distributions to be responsible for the observed BaO* signal. Although the excitation function for the title reaction is yet unknown, it is often found in exoergic reactions like the chemiluminescent channel of Ba($^1S_0$)+N_2O,[41] for the cross section to decrease significantly as the collision energy increases as a result of a number of dynamical factors including the shorter interaction time, recrossing,[4] or the opening of alternative, endoergic removal processes. Some possible removal processes for the present system are collision-induced dissociation and collisional ionization (see Sec. III A), with calculated thresholds of 5.85 and 11.55 eV, respectively, using D(N_2–O) =1.74 eV,[33] a Ba($^1S_0$) ionization potential of 5.21 eV,[42] and a N_2O vertical electron affinity (VEA) of −2.23 eV.[43] The latter threshold, along with the possible production of BaO^+ above 6.91 eV, suggests that a broad range of collision energies could lead to reaction, especially considering the high efficiency of the Ba(^3P) beam source.

Conclusions derived from a comprehensive analysis of the whole data series here certainly indicate a dominant $A\ ^1\Sigma^+ \rightarrow X\ ^1\Sigma^+$ contribution to chemiluminescence. This does not mean that the remaining 2 eV states or higher-lying states are not populated at all in the present reaction. Instead, it may show an absence of preferential production of such BaO excited states regarding $A\ ^1\Sigma^+$. In such a case, drift of the longer-lived $A'\ ^1\Pi$, $a\ ^3\Sigma^+$, and $b\ ^3\Pi$ state products out of the field of view could significantly contribute to the lack of observation of the corresponding fluorescence. Indeed, the estimate of 99/1 for the $A-X$ to $A'-X$ intensity ratio in Sec. III A corresponds to a value of $\Gamma(A/A')=0.005$, which appears much too small to be accounted for on the basis of flyout effects alone. The lack of evidence for chemiluminescence from highly excited BaO states, especially the short-lived $C\ ^1\Sigma^+$ state, is difficult to rationalize on these grounds, which suggests that the mechanism for the present reaction may exhibit dynamic constraints regarding orbital occupation. The nature of such a mechanism is discussed hereafter. The relatively large values of $\langle P_2(J' \cdot \hat{k}) \rangle_{av}$ for the BaO($A\ ^1\Sigma^+$) product found here and elsewhere[8] in the unconstrained Ba(^3P)+$N_2O \rightarrow$ BaO*+N_2 reaction system at the hyperthermal collision energies studied suggest a direct mechanism, which is further supported by the high rotational and, particularly, vibrational excitations of the BaO($A\ ^1\Sigma^+$) product.

Since the BaO($A\ ^1\Sigma^+$) product formed has a single charged Ba^+O^- character,[17,18] avoided ionic-covalent curve crossings have been inferred previously[8] from the finding of a negative correlation between the BaO($A\ ^1\Sigma^+$) rotational alignment and its vibrational state, such as that derived here at $\langle E_c \rangle$=7.47 eV. Within a "multilocation harpoon" picture[2] of the reaction mechanism, the outermost ionic-covalent crossing corresponds to the ground-state $Ba^+(6s\ ^2S_{1/2}) \cdots N_2O^-$ [$^2\Pi$ ($^2A'$ in C_s symmetry)] ionic surface. The latter correlates adiabatically (spin disregarded) with several energetically accessible excited states of BaO: with $A\ ^1\Sigma^+$ and $a\ ^3\Sigma^+$ in C_s, and with $A'\ ^1\Pi$ and $b\ ^3\Pi$ in C_{2v}.[41] Direct formation of the BaO($A\ ^1\Sigma^+$) product requires a spin-flip in the ion-pair intermediate, a process that would be favored by a long-lived complex which, in turn, seems incompatible with the direct character of the present reaction. Alternatively, the BaO($A\ ^1\Sigma^+$)+$N_2(^1\Sigma_g^+)$ singlet surface may be reached through mixings in the exit channel with potential energy surfaces (PESs) leading to the BaO($a\ ^3\Sigma^+, b\ ^3\Pi$) +$N_2(^1\Sigma_g^+)$ triplet surfaces, following access to the latter by charge transfer at the outer ionic-covalent crossing. As discussed previously,[8] this mechanism appears very plausible owing to the extensive perturbations that occur[17] among the $A\ ^1\Sigma^+$, $b\ ^3\Pi$, and $A'\ ^1\Pi$ states, as well as the $A'\ ^1\Pi$ and $a\ ^3\Sigma^+$ states of BaO. It is also substantiated by analyzing the valence orbital configuration of the $A\ ^1\Sigma^+/a\ ^3\Sigma^+$ and $A'\ ^1\Pi/b\ ^3\Pi$ electronic states, i.e., [Ba($6s\sigma$)O($2p\sigma 2p\pi^4$)] and [Ba($6s\sigma$)O($2p\sigma^2 2p\pi^3$)],[18] respectively, which suggest that the $Ba^+(6s) \cdots N_2O^-$ intermediates could decay to products without orbital rearrangement. In contrast, population of the 4 eV electronic states, which involves excitations of $p\pi$ or $5d$ orbitals located on Ba,[19] would require significant orbital rearrangement of the intermediate and, given that the 2 eV and the 4 eV states do not perturb to each other, the apparent lack of production in such states indicates some degree of orbital control that could be involved in the exit channel of the reaction, at least.

The indiscernible variation of $\langle P_2(J'\cdot\hat{k})\rangle$ with the BaO* vibrational levels that is found at 4.82 eV suggest that most of the relevant reactive encounters sample more similar collision geometries in comparison with the two higher $\langle E_c\rangle$, and the higher rotational alignments of the former further indicate that correspondingly higher geometric constraints are operative. Since N_2O bending is expected to play an increasing role in the reaction intermediates at the relatively lower collision energies (and thus higher collision times) of the lowest $\langle E_c\rangle$, coplanar (C_s) approach of Ba to the "O-end" of bent N_2O is likely to be favored over collinear attack on linear (equilibrium) N_2O. A related approach-geometry limitation having also comparable magnitudes at both thermal and hyperthermal collision energies has been considered by Wiskerke *et al.*[4] to account for steric effects in the harpoon $K+CH_3I\rightarrow KI+CH_3$ reaction. They proposed the existence of an approach angle-dependent potential barrier which arises from the ionic-covalent crossing occurring on the repulsive region of the covalent potential, and whose effective height increases with the specific E_c that is sampled by any particular reactive trajectory. At least at thermal collision energies, an angle-dependent barrier is also expected in the present reaction by comparison with two models[44,45] for the related chemiluminescent channel involving $Ba(^1S_0)$, which were previously proposed on the basis of very detailed attack orientation-controlled experiments.[39,46] Corroboration of such proposal would actually require the ability to orient the N_2O, which is not feasible in the current experiments. Yet it is plausible that the stereodynamics observed at 4.82 eV stems from a potential barrier to reaction which favors charge transfer at chiefly coplanar geometries. In such a case, some significant alignment of BaO* rotation perpendicular to k could ensue any product repulsion at threshold if the reactant orbital angular momentum L is much larger than the rotational angular momentum of N_2O, J_{N_2O}, as it is likely to hold[8] under the current experimental conditions.

Following Wiskerke *et al.*,[4] any involvement of ionic-covalent crossings here is expected to give rise to substantial barriers owing to the large negative VEA of N_2O in its ground vibrational state (most populated at 298 K). A simple Magee-type calculation[47] yields a crossing radius R_c from the $Ba(^3P)\cdots N_2O$ curve to the ground-state $Ba^+(^2S_{1/2})\cdots N_2O^-$ ionic surface [$Ba(^3P)$ ionization potential: 3.59 eV] (Ref. 42) of 2.47 Å. Considering Ba approach towards the N_2O centre-of-mass perpendicular to its internuclear axis, the Ba···O distance is predicted to be ~2.71 Å which, compared to the sum of the Ba and O van der Waals radii, 4.60 Å,[48] suggests that charge transfer will occur well within the repulsive region. Additional repulsion is anticipated in this case owing to the π electron distribution in $N_2O(^1\Sigma^+)$. Moreover, as this geometry evolves into perfect ($C_{\infty v}$) O-end attack on N_2O, the system should start to experience repulsion at progressively shorter Ba···O distances. In this context, inner crossings with excited ionic surfaces [$Ba^+(5d\ ^2D_J, 6p\ ^2P_J, \cdots)$] seem unlikely to contribute as they will be shifted further into the repulsive region.

Similar considerations apply to any reactive encounter involving N_2O in its first excited bending level ($n_2=1$), as a recent high-level *ab initio* study[49] on the N_2O dissociative electron attachment (DEA) reports a small difference (by about 50 meV) between the N_2O VEAs associated with the $n_2=0$ (ground-state) and $n_2=1$ bending levels. Thus, unlike the $K+CH_3I$ reaction,[4] no significant change in the height and location of the reaction barrier proposed here is expected to accompany the decreasing role that bent N_2O configurations would play at elevated collision energies.

As pointed out before,[8] the major dynamical limitation would instead arise from the charge transfer (and consequently the reaction) having a larger probability when the collision time is higher than the time needed for N_2O bending. A recent DEA study[49] on N_2O suggests that dissociation of N_2O^- is delayed selectively by an avoided crossing between the $^2A'$ surface that leads to direct N_2+O^- dissociation and an $^2A''$ bound surface that corresponds in the dissociation limit to N_2^-+O, since the coupling between these two surfaces is both strongest for linear N_2O and strongly dependent on the N–N–O bond angle. Indeed, this seems suitable to account for the collision energy-dependent correlation between the rotational alignment of $BaO(A\ ^1\Sigma^+)$ and its vibrational levels observed here. Namely, at any particular $\langle E_c\rangle$, only collisions between Ba and N_2O having E_c at or above the proposed reaction threshold will lead to reaction. Geometric requirements at threshold should be rather stringent. For an initial covalent interaction, a preference for collinear/coplanar O-end approach of Ba at low impact parameters is to be expected in order to favor overlapping of the $6p$ orbital of $Ba(^3P)$ with the $3\pi/10a'$ orbital of linear/bent N_2O. Both collision geometries would lead to substantial BaO* rotational alignment, and for the coplanar case a wider, unspecific vibrational population would be favored owing to the Ba^+-O^- attraction beginning earlier in the PES. Hence the alignment results at $\langle E_c\rangle=4.82$ eV can be rationalized on the basis of the corresponding narrower distribution of collision energies by assuming that a sizeable potential barrier is operative for most of the reactive trajectories.

For the reactive intermediates involving bent N_2O, $\langle P_2(J'\cdot\hat{k})\rangle$ should fall with rising collision energies as a result of an increasing tendency of k to lie outside the reaction plane. Along with the predicted prevalence as E_c raises of collinear reactive intermediates, the insensitivity of the BaO rotational alignment to its vibrational state at 4.82 eV would be expected to develop into the observed negative correlation between $\langle P_2(J'\cdot\hat{k})\rangle$ and v' at the two higher $\langle E_c\rangle$.

In this context the falling $\langle P_2(J'\cdot\hat{k})\rangle_{av}$ values with increasing $\langle E_c\rangle$ could be due to the development at the two highest, hyperthermal $\langle E_c\rangle$ studied here of so-called "induced repulsive energy release,"[50] following relaxation of the collision partners from compressed and bent configurations which do not occur at thermal energies and that are expected to scramble any product rotational alignment.

To support the above picture for the present reaction dynamics, the $BaO(A\ ^1\Sigma^+)$ rotational alignment was calculated by using a simplified version[11] of the generalized electron-jump DIPR-DIP model.[12] Both models are suitable to account for the product rotational alignment in beam-gas chemiluminescent reactions of the type $A+BC\rightarrow AB^*+C$

where repulsive energy releases impulsively as products separate. The latter would seem reasonable to assume here on the basis of previous modeling by Stolte and coworkers[45] of $\langle P_2(J'\cdot\hat{k})\rangle$ data for the chemiluminescent Ba($^1S_0$)+N_2O reaction from nonrandom collision experiments. In combining another simplified DIPR theory with the angle-dependent line of normals model, they found the experimental results to be consistent with an impulsive and large (of the order of an eV) repulsive energy release. The DIPR-DIP model used presently[11] incorporates three simplifications to the generalized formulation,[12] namely, that

(1) the repulsive energy is released instantaneously, which could be a good assumption here according to the modeling results[45] on the Ba($^1S_0$)+N_2O reaction;
(2) the reaction probability is unity for reagent impact parameters $b's \leq R_c$ (the results are thus independent of R_c), which may be the case only at the lowest $\langle E_c\rangle$ studied here where the system is less susceptible to a failure of the charge transfer to occur;
(3) the probability of collision between A and BC is isotropic; this is likely a crude assumption, given the shape of N_2O, where intuitively reaction is expected to depend upon approach angle.

Within the model,[11] formulation of $\langle P_2(J'\cdot\hat{k})\rangle = [3\langle(J'\cdot\hat{k})^2\rangle]/2$, is made by identifying $(J'\cdot\hat{k})$, i.e., the cosine of the angle between the product rotational angular momentum J' and k, with the projection of J' along z. The latter is a function of only b and the Euler angles (ϕ,θ,χ) describing the coordinates of BC, and it also depends on the repulsive release of energy R through the following reduced parameter:

$$\lambda = \frac{m_B\langle k\rangle}{\sqrt{2R\mu_{BC}}}, \tag{3}$$

where m_B and μ_{BC} are the mass of B and the BC reduced mass, respectively. R may be estimated by[51]

$$R = \mathrm{EA(B)} - \mathrm{D(BC)} - \mathrm{EA(BC)}, \tag{4}$$

where EA(B) is the electron affinity of B, and D(BC) and EA(BC) are the dissociation energy and the electron affinity of BC, respectively. Calculation of $\langle P_2(J'\cdot\hat{k})\rangle$ then involves a simple average of $(J'\cdot\hat{k})^2$ over the distribution of J' about z.[11] A further motivation for using this model is that it is largely independent of any assignment of the BaO* emitters, so the results of its application will remain valid also when an improved spectroscopic characterization of the chemiluminescence spectra is available.

Table IV shows the results of a DIPR-DIP calculation using $R=1.99$ eV, obtained from Eq. (4) with EA(O) $=1.46$ eV,[33] $D(N_2-O)=1.74$ eV, and EA(N_2O) $=-2.23$ eV. With the exception of the datum at $\langle E_c\rangle = 4.82$ eV, it is apparent that the DIPR-DIP model alignment disagrees with both the magnitude and the velocity dependence of the experimental alignment. The latter is not surprising since the basic assumptions of the DIPR-DIP model favor conversion of collision energy into polarization of the product rotation perpendicular to k.[12] Instead, the present calculations qualitatively show that dynamical factors, other than repulsive release of energy, most likely time-scale constraints on the charge transfer and/or induced repulsive energy release, control the angular momentum disposal at the hyperthermal $\langle E_c\rangle$ studied. Clearly, further exploration of this suggestion will require carrying out dynamical calculations on accurate four-body PES. This is particularly true at the hyperthermal collision energies studied here, where time-scale constraints on charge transfer and/or induced repulsive energy release may become dominant over repulsive energy release.

The substantial energy deficits E_d and $E_{tot}-E_B$ at all $\langle E_c\rangle$ studied (see Table III) are by no means unique to the present reaction. Indeed, large energy deficits, i.e., in the range of 0.5–3.7 eV, appear to be a common feature of group 2 metal atoms plus N_2O reactions even at thermal collision energies.[15,24,52–55] This has been generally ascribed to vibrational excitation of the N_2 product, though recent experimental[56] and theoretical[49] DEA investigations on the isolated system N_2O/N_2O^- instead suggest that much more energy is transferred in N_2 rotation than both in its vibration and in product relative translation. The latter explanation would seem reasonable in the scenario of the present gas-phase reaction given the apparent key role that is played by N_2O bending. Moreover, substantial energy released as N_2 rotation and product translation is what could be expected[50] from the above-suggested involvement of induced repulsive energy release. This further suggests an interesting speculation for the apparent lack of production of BaO excited states at 4 eV from an energetic standpoint: That the N_2 product takes too much of the total product energy, thus preventing formation of these states. In any case, substantial energy deficits here may well be the consequence of the fact that, at all $\langle E_c\rangle$, the total product energy is sufficient to allow formation of nonemitting both BaO Rydberg states and products of dissociation Ba+O+N_2 as well as collisional ionization $Ba^+ + N_2O^-$.

V. CONCLUSIONS

The energy and angular momentum disposal in the chemiluminescent reaction Ba(^3P)+N_2O were investigated under hyperthermal beam-Maxwellian gas conditions at the three specific average collision energies of 4.82, 5.85, and 7.47 eV. The fully dispersed polarized chemiluminescence spectra revealed that the BaO($A\ ^1\Sigma^+$) product rotational alignment is insensitive to its vibrational state v' at $\langle E_c\rangle = 4.82$ eV and develops into an increasingly negative correlation between $\langle P_2(J'\cdot\hat{k})\rangle$ and v' as $\langle E_c\rangle$ is raised. Such behavior is interpreted in terms of a mechanism involving a short-range, partial electron transfer from Ba(^3P) to N_2O which is constrained by the duration of the collision, so that the reaction has a larger probability when the N_2O has time enough to bend during the collision. The latter in turn determines that, at any given $\langle E_c\rangle$, collinear reactive intermediates are preferentially involved when the highest velocity components of the corresponding collision energy distributions are sampled. Moreover, the data at 4.82 eV suggest that a poten-

tial barrier to reaction which favors charge transfer to bent N_2O at chiefly coplanar geometries is operative for most of the reactive trajectories that sample the lowest velocity components. Such a barrier would arise from the relevant ionic-covalent curve crossings occurring in the repulsive region of the covalent potential $Ba(^3P)\cdots N_2O(^1\Sigma^+)$; from this crossing the $BaO(A\ ^1\Sigma^+)$ product may be reached through mixings in the exit channel with PESs leading most likely to the spin-allowed $b\ ^3\Pi$ and $a\ ^3\Sigma^+$ products.

At all $\langle E_c\rangle$, the significant magnitude of the average $BaO(A\ ^1\Sigma^+)$ rotational alignments obtained, and the high $BaO(A\ ^1\Sigma^+)$ rovibrational excitations that derive from spectral simulations of the unpolarized chemiluminescence spectra both indicate that the reaction mechanism is predominantly direct, and consistently point to dynamic factors other than time-scale constraints, most likely the development of induced repulsive energy release, as the major responsible for their variation with increasing $\langle E_c\rangle$. A simplified version of the DIPR-DIP model does not give agreement with the observed $\langle P_2(J'\cdot\hat{k})\rangle_{av}$ values. This may attributed to the fact that the model oversimplifies the reaction dynamics, by ignoring the four-body PES. The present work suggests that it will be necessary to carry out dynamical calculations on a realistic PES for the reaction in order to account for the $\langle P_2(J'\cdot\hat{k})\rangle_{av}$ data as a function of $\langle E_c\rangle$. This is particularly true at the hyperthermal collision energies studied here, where time-scale constraints on charge transfer and/or induced repulsive energy release may become dominant over the repulsive release of energy.

ACKNOWLEDGMENTS

We thank CONICET, FONCYT, and ACC for financial support. One of us (M.R.) acknowledges a doctoral fellowship from CONICET-Argentina.

[1] M. Polanyi, *Atomic Reactions* (Williams and Northgate, London, 1932).
[2] J. M. Mestdagh, B. Soep, M. A. Gaveau, and J. P. Visticot, Int. Rev. Phys. Chem. **22**, 285 (2003).
[3] K. C. Lin and A. González Ureña, Int. Rev. Phys. Chem. **26**, 289 (2007).
[4] A. E. Wiskerke, S. Stolte, H. J. Loesch, and R. D. Levine, Phys. Chem. Chem. Phys. **2**, 757 (2000).
[5] M. De Castro, R. Candori, F. Pirani, V. Aquilanti, M. Garay and A. González Ureña, J. Chem. Phys. **112**, 770 (2000) (and Refs. 5 and 6 therein).
[6] M. A. Spence, W. R. Tomlinson, and M. R. Levy, Phys. Chem. Chem. Phys. **3**, 3622 (2001) (and references of the senior author therein).
[7] M. A. Spence, W. R. Tomlinson, and M. R. Levy, Phys. Chem. Chem. Phys. **3**, 3610 (2001).
[8] M. Rossa, C. A. Rinaldi, and J. C. Ferrero, J. Chem. Phys. **127**, 064309 (2007).
[9] M. Rossa, C. A. Rinaldi, and J. C. Ferrero, J. Appl. Phys. **100**, 063305 (2006).
[10] M. Rossa, C. A. Rinaldi, and J. C. Ferrero, J. Appl. Phys. **105**, 063306 (2009).
[11] G. Ding, W. Yang, W. Sun, D. Xu, G. He, and N. Lou, Chem. Phys. Lett. **220**, 1 (1994).
[12] M. G. Prisant, C. T. Rettner, and R. N. Zare, J. Chem. Phys. **81**, 2699 (1984).
[13] B. M. Miles and W. L. Wiese, At. Data **1**, 1 (1969).
[14] R. C. Estler and R. N. Zare, Chem. Phys. **28**, 253 (1978).
[15] J. W. Cox and P. J. Dagdigian, J. Chem. Phys. **79**, 5351 (1983).
[16] C. Alcaraz, P. de Pujo, J. Cuvellier, and J. M. Mestdagh, J. Chem. Phys. **89**, 1945 (1988).
[17] R. A. Gottscho, P. S. Weiss, R. W. Field, and J. G. Pruett, J. Mol. Spectrosc. **82**, 283 (1980).
[18] R. A. Gottscho, J. B. Koffend, and R. W. Field, J. Mol. Spectrosc. **82**, 310 (1980).
[19] D. Bender, S. H. Schaefer, and E. Tiemann, J. Mol. Spectrosc. **116**, 286 (1986).
[20] N. Furio and J. G. Pruett, J. Mol. Spectrosc. **136**, 120 (1989).
[21] H. Li, C. Focsa, B. Pinchemel, R. J. Le Roy, and P. F. Bernath, J. Chem. Phys. **113**, 3026 (2000).
[22] J. J. Reuther and H. B. Palmer, J. Chem. Phys. **77**, 83 (1982).
[23] J. M. Mestdagh, P. Meynadier, P. de Pujo, O. Sublemontier, J. P. Visticot, C. Alcaraz, J. Berlande, and J. Cuvellier, Chem. Phys. Lett. **164**, 5 (1989).
[24] M. de Castro, C. Rinaldi, L. M. Gamo, J. Cáceres, and A. González Ureña, Phys. Chem. Chem. Phys. **2**, 4115 (2000).
[25] J. G. Pruett and R. N. Zare, J. Chem. Phys. **62**, 2050 (1975).
[26] S. E. Johnson, J. Chem. Phys. **56**, 149 (1972).
[27] R. A. Gottscho, J. B. Koffend, R. W. Field, and J. R. Lombardi, J. Chem. Phys. **68**, 4110 (1978).
[28] Y. C. Hsu, B. Hegemann, and J. G. Pruett, J. Chem. Phys. **72**, 6437 (1980).
[29] A. L. G. Rees, Proc. Phys. Soc. London **59**, 998 (1947).
[30] R. J. Le Roy, RKR1, University of Waterloo Chemical Physics Research Report No. CP-425, 1992; R. J. Le Roy, LEVEL 7.0, University of Waterloo Chemical Physics Research Report No. CP-642, 2000. The source codes and manuals for both programs were obtained from the www site http://leroy.uwatwerloo.ca.
[31] R. W. Field, G. A. Capelle, and M. A. Revelli, J. Chem. Phys. **63**, 3228 (1975).
[32] W. H. Parkinson, Proc. Phys. Soc. London **78**, 705 (1961).
[33] *CRC Handbook of Chemistry and Physics, Internet Version 2007*, 87th ed., edited by D. R. Lide (Taylor and Francis, Boca Raton, FL, 2007).
[34] G. Herzberg, *Molecular Spectra and Molecular Structure* (Van Nostrand Reinhold, New York, 1950).
[35] J. Cuvellier, P. de Pujo, J. M. Mestdagh, P. Meynadier, J. P. Visticot, J. Berlande, and A. Binet, J. Chem. Phys. **90**, 7050 (1989).
[36] J. P. Visticot, C. Alcaraz, J. Berlande, J. Cuvellier, T. Gustavsson, J. M. Mestdagh, P. Meynadier, P. de Pujo, and O. Sublemontier, J. Chem. Phys. **94**, 4913 (1991).
[37] M. G. Prisant, C. T. Rettner, and R. N. Zare, J. Chem. Phys. **75**, 2222 (1981).
[38] M. A. Spence and M. R. Levy, J. Phys. Chem. **101**, 7490 (1997).
[39] H. Jalink, G. Nicolasen, S. Stolte, and D. H. Parker, J. Chem. Soc., Faraday Trans. 2 **85**, 1115 (1989).
[40] Z. Wang, G. He, and N. Lou, Chem. Phys. Lett. **147**, 116 (1988).
[41] D. J. Wren and M. Menzinger, Faraday Discuss. Chem. Soc. **67**, 97 (1979).
[42] NIST database, http://webbook.nist.gov.
[43] D. G. Hopper, A. C. Wahl, R. L. C. Wu, and T. O. Tiernan, J. Chem. Phys. **65**, 5474 (1976).
[44] A. González Ureña, Nuovo Cimento D **11**, 1389 (1989).
[45] G. T. Evans, E. van Kleef, and S. Stolte, J. Chem. Phys. **93**, 4874 (1990).
[46] D. H. Parker, H. Jalink, and S. Stolte, Faraday Discuss. Chem. Soc. **84**, 184 (1987).
[47] J. L. Magee, J. Chem. Phys. **8**, 687 (1940).
[48] S. S. Batsanov, Inorg. Mater. **37**, 871 (2001).
[49] H. U. Suter and T. Greber, J. Phys. Chem. B **108**, 14511 (2004).
[50] A. M. G. Ding, L. J. Kirsch, D. S. Perry, J. C. Polanyi, and J. L. Schreiber, Faraday Discuss. Chem. Soc. **55**, 252 (1973).
[51] D. Herschbach, Faraday Discuss. Chem. Soc. **55**, 233 (1973).
[52] C. D. Jonah, R. N. Zare, and Ch. Ottinger, J. Chem. Phys. **56**, 263 (1972).
[53] J. A. Irvin and P. J. Dagdigian, J. Chem. Phys. **74**, 6178 (1981).
[54] P. J. Dagdigian, J. Chem. Phys. **76**, 5375 (1982).
[55] J. W. Cox and P. J. Dagdigian, J. Phys. Chem. **86**, 3738 (1982).
[56] M. Allan and T. Skalický, J. Phys. B **36**, 3397 (2003).